Analytical approach for nonlinear vibration response of the thin cylindrical shell with a straight crack

Tong Wang
Zhejiang University of Technology
Chengyan Wang
Zhejiang University of Technology
Yaxing Yin
Zhejiang University of Technology
Yankang Zhang
Zhejiang University of Technology
Lin Li
Zhejiang University of Technology
Dapeng Tan (tandapeng@zjut.edu.cn)
Zhejiang University of Technology https://orcid.org/0000-0002-6018-9648

Research Article

Keywords: Thin cylindrical shells, straight crack, nonlinear vibration response, local flexibility, crack identification

Posted Date: September 30th, 2022

DOI: https://doi.org/10.21203/rs.3.rs-2076936/v1

Analytical approach for nonlinear vibration response of the thin cylindrical shell with a straight crack

Tong Wang[a], Chengyan Wang[a], Yaxing Yin[a], Yankang Zhang[a], Lin Li[a,b], Dapeng Tan[a,b,1]

[a] *College of Mechanical Engineering, Zhejiang University of Technology, 310014 Hangzhou, PR China*

[b] *Collaborative Innovation Center of High-end Laser Manufacturing Equipment, Zhejiang Province & Ministry of Education, 310014 Hangzhou, PR China*

ABSTRACT: Thin cylindrical shells are susceptible to cracking under long-term load and external impact, and it is of considerable scientific and technical value to investigate the nonlinear vibration response characteristics and monitor the health condition of the shell structure. Based on the Flügge shell theory, the nonlinear dynamic model for the thin cylindrical shell is established. By the partial Fourier transform combined with the residue theorem, the forced vibration generation and propagation mechanism of the thin cylindrical shell are investigated, and the analytical solution of forced vibration displacement in the space domain is obtained. Then, the local flexibility matrix is derived from the perspective of fracture mechanics, and the continuous coordination condition on both sides of the straight crack is constructed using the Linear Spring Model (LSM). Combined with the wave superposition principle, the analytical approach for nonlinear vibration response is proposed to reveal the evolution law of vibration characteristics of the thin cylindrical shell with a straight crack, and then a straight crack identification method based on natural frequency isolines and amplitude maximization methods is presented. Finally, the effect of various morphological information of the straight crack on the nonlinear vibration response characteristics of the thin cylindrical shell is studied in detail, and a numerical case is conducted to verify the effectiveness of the proposed straight crack identification method.

Keywords: *Thin cylindrical shells; straight crack; nonlinear vibration response; local flexibility; crack identification*

1 Introduction

With the continuous development of modern industrial technology, thin cylindrical shells have been widely applied in petrochemical engineering, pipeline transportation, aerospace, civil engineering, and other engineering fields due to

[1]Corresponding author
E-mail: tandapeng@zjut.edu.cn (Dapeng Tan), Tel: +86-13858046218.

their excellent mechanical properties and structural characteristics [1-3]. However, in countless application scenarios, the thin cylindrical shell is subjected to sustainable external excitation and violent impact, forcing the thin cylindrical shell to produce nonlinear vibration and noise, which can easily cause damage to the shell structure and even fatigue fracture, posing a threat to life and property safety [4,5], as shown in Fig.1. Moreover, the nonlinear vibration characteristics of the thin cylindrical shell are complicated, and the coupling between circumferential and axial modes needs to be considered, which increases the difficulty of modeling and solving. And because the nonlinear component and discontinuous propagation of force and displacement caused by straight crack are challenging to be described by an accurate mathematical model, the nonlinear vibration characteristics and crack identification techniques of the thin cylindrical shell have not been extensively studied. Therefore, it is necessary to propose the analytical approach for nonlinear vibration response of the thin cylindrical shell with a straight crack, reveal the generation and propagation mechanism of forced vibration and the evolution law of nonlinear vibration response, and then develop a shell structure health monitoring technology that can detect, evaluate and locate crack damage in time.

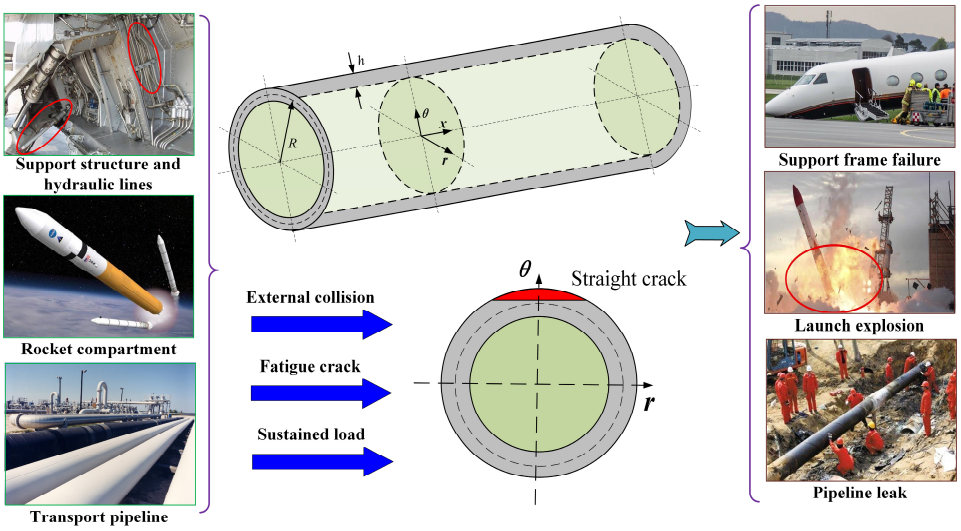

Fig. 1. Typical engineering applications and crack damage of thin cylindrical shells.

The thickness of the thin cylindrical shell is small compared with other geometric dimensions (radius, length, etc.). When the shell vibrations are generated by external excitations, their circumferential modes significantly impact the nonlinear vibration response. Therefore, the nonlinear coupling effect of circumferential and axial modes should be considered in studying the vibration response of the thin cylindrical shell. Flügge established the free vibration displacement equations with the mid-surface element as the research object, proposed the wave propagation method to solve these equations, obtained the relationship between the dimensionless frequency and energy distribution, and analyzed the propagation properties of complex waves in low-order circumferential modes [6,7]. Sorokin adapted the wave propagation method to analyze the dispersion characteristics of

the helically orthotropic cylindrical shells and revealed the energy distribution under rotational excitation [8]. Wang simplified the boundary conditions of orthotropic cylindrical shells by using the wave propagation method, explored the natural vibration frequency characteristics under different boundary conditions, and analyzed the influence of geometric and physical parameters on the frequency characteristics of cylindrical shells under axial pressure [9]. Arbind studied the nonlinear kinematic characteristics of isotropic hyperelastic shells based on the general higher-order shell theory under quasi-static conditions [10]. In addition, Zhang[11], Guo[12], Liu[13], Amabili[14], and others studied the nonlinear vibration response and sound radiation characteristics of underwater cylindrical shells, partially submerged cylindrical shells, functionally graded material sandwich cylindrical shells, and truncated conical shells, and made a series of achievements, providing the theoretical basis for vibration and noise reduction of relevant equipment. However, the relevant research focuses on the inherent characteristics of the thin cylindrical shell from the perspectives of wave propagation and energy [15-17], and little literature gives specific analytical solutions for the forced nonlinear vibration displacement response of the thin cylindrical shell.

The straight crack is one of the most common defects in any type of shells and plates. Rapid external impact and excessive bending of the thin cylindrical shell are more likely to produce the straight crack, resulting in changes in structural parameters and mechanical vibration characteristics [18]. The straight crack is more likely to form stress concentration under the action of bending moment, leading to crack propagation and even fracture. Therefore, it is necessary to explore the nonlinear vibration response characteristics of the thin cylindrical shell with a straight crack and complete the straight crack identification in the thin cylindrical shell. At present, the crack damage detection methods based on vibration response characteristics mainly focus on circumferential crack of the thin cylindrical shell or part-through crack of plate and beam [19,20]. There is no report on the damage detection of the straight crack, which is related to the complexity of the stress intensity factor (SIFs) of straight crack sections, the solution of local flexibility coefficients and the nonlinear vibration response. Using a rotating spring to simulate cracks, Naniwadekar proposed a pipeline crack identification method based on natural frequency to predict the circumferential position and the crack depth based on the change rate of natural frequency, but the axial position cannot be obtained [21]. Moradi divided the circumferential cracked shells into four parts, and the crack was simulated by line spring. The natural frequency of cracked shells was obtained using the differential quadrature method for the characteristic value analysis. According to the corresponding relationship between crack parameters and natural frequency, the location, length, and depth of the crack could be better predicted [22]. Zhang proposed a crack identification method for cylindrical shells based on the frequency shift curve. The trough with the minimum value represents

the circumferential position of the damage, and the difference between the lowest trough value and the three trough values can be conducted to describe the damage degree [23]. Assuming that the crack length was much smaller than the curvature radius of the shells, Moazzez adapted the two-dimensional linear spring theory to simplify the crack area into a flat plate and directly established the nonlinear relationship between the near-field and far-field forces. Meanwhile, the nonlinear coupling effect between far-field forces and moments is ignored by adding a local flexibility coefficient to obtain the relationship between the crack parameters and the natural frequency [24,25]. For the non-whole circumferential crack, the existing literature has not identified all the crack morphological information (length, depth, location and circumferential position).

Given the above matters, this paper aims to solve the local flexibility coefficients of the straight crack, explore the generation and propagation mechanism of forced nonlinear vibration response, and put forward an analytical approach for the nonlinear vibration response of the thin cylindrical shell with a straight crack. According to the nonlinear vibration response characteristics of the thin cylindrical shell with a straight crack, a nonlinear vibration signal identification method for straight crack damage is proposed. The rest of this paper is organized as follows. In Section 2, the solution equations of the local flexibility matrix of the straight crack are derived, and the Linear Spring Model (LSM) is conducted to construct the continuous coordination conditions on both sides of a straight crack. Combined with residual theorem and wave superposition principle, an analytical method for nonlinear vibration response of the thin cylindrical shell with a straight crack and a straight crack identification method based on natural frequency isolines and amplitude maximization methods are presented. In Section 3, the accuracy of the critical factors in the solution process and the correctness of the proposed analytical approach for nonlinear vibration response are verified by comparing the analytical results with experimental, literature, and finite element model (FEM) results. In Section 4, the nonlinear vibration response characteristics of the thin cylindrical shell without or with a straight crack are discussed and analyzed to reveal the evolution law of the natural frequency and forced vibration displacement response under different straight crack morphology and the correctness of the proposed straight crack identification method is verified by an engineering case. In Section 5, the conclusions are obtained.

2 Theoretical formulation

2.1 Nonlinear dynamic model of the thin cylindrical shell

The nonlinear vibration response of the thin cylindrical shell is the basis of this study. According to Flügge shell theory, the nonlinear dynamic model of the thin

cylindrical shell is established, as shown in Fig.1. Assuming that u, v, and w represent the axial, circumferential, and radial displacement, R is the radius of the midplane, and h is the shell thickness, the free vibration displacement equations of the thin cylindrical shell based on the theory of elastomer stress and strain are described as [26]:

$$\left(R^2\frac{\partial^2}{\partial x^2}+(1+\beta^2)\frac{1-\mu}{2}\frac{\partial^2}{\partial\theta^2}\right)u+\left(R\frac{1+\mu}{2}\frac{\partial^2}{\partial x\partial\theta}\right)v+\left(R\mu\frac{\partial}{\partial x}-R^3\beta^2\frac{\partial^3}{\partial x^3}+R\beta^2\frac{1-\mu}{2}\frac{\partial^3}{\partial x\partial\theta^2}\right)w=R^2\rho\frac{1-\mu^2}{E}\frac{\partial^2 u}{\partial t^2} \tag{1}$$

$$\left(R\frac{1+\mu}{2}\frac{\partial^2}{\partial x\partial\theta}\right)u+\left(R^2\frac{1-\mu}{2}\frac{\partial^2}{\partial x^2}+\frac{\partial^2}{\partial\theta^2}+3R^2\beta^2\frac{1-\mu}{2}\frac{\partial^2}{\partial x^2}\right)v+\left(\frac{\partial}{\partial\theta}-R^2\beta^2\frac{3-\mu}{2}\frac{\partial^3}{\partial x^2\partial\theta}\right)w=R^2\rho\frac{1-\mu^2}{E}\frac{\partial^2 v}{\partial t^2} \tag{2}$$

$$\left(R\mu\frac{\partial}{\partial x}-R^3\beta^2\frac{\partial^3}{\partial\theta^3}+R\beta^2\frac{\partial^3}{\partial x\partial\theta^2}\right)u+\left(\frac{\partial}{\partial\theta}-R^2\beta^2\frac{3-\mu}{2}\frac{\partial^3}{\partial x^2\partial\theta}\right)v+\left(1+\beta^2+\beta^2\Delta^2+2\beta^2\frac{\partial^2}{\partial\theta^2}\right)w=-R^2\rho\frac{1-\mu^2}{E}\frac{\partial^2 w}{\partial t^2} \tag{3}$$

where ρ is the material density, the thickness of the factor β^2 is expressed as $\beta^2=\frac{h^2}{12R^2}$, μ is Poisson's ratio, E is the Young modulus, and $\Delta=R^2\left(\frac{\partial^2}{\partial x^2}+\frac{\partial^2}{\partial\theta^2}\right)$ is the Laplace operator in cylindrical coordinates.

Considering the nonlinear coupling effect between circumferential and axial modes, the wave propagation method is adopted to solve the migration solution of the free vibration equation, which can be described as [27,28]:

$$\begin{cases} u=\sum_{n=0}^{\infty}\sum_{s=1}^{\infty}U_{ns}\cos(n\theta)\exp\left[i(\omega t-k_{ns}x)\right] \\ v=\sum_{n=0}^{\infty}\sum_{s=1}^{\infty}V_{ns}\sin(n\theta)\exp\left[i(\omega t-k_{ns}x)\right] \\ w=\sum_{n=0}^{\infty}\sum_{s=1}^{\infty}W_{ns}\cos(n\theta)\exp\left[i(\omega t-k_{ns}x)\right] \end{cases} \tag{4}$$

where k_{ns} is the axial wave number, ω is the circular frequency of the axial wave, n is the circumferential mode number, s is the half-wave number in the axial direction, $\exp(i\omega t)$ is the time factor, U_{ns}, V_{ns}, and W_{ns} are the axial, circumferential, and radial displacement amplitude. For the clamped-clamped boundary condition, the axial wave number is $k_{ns}=\frac{(2m+1)\pi}{2L}$. For the simple supported-simple supported boundary condition, the axial wave number is $k_{ns}=\frac{m\pi}{L}$.

In solving the displacement response of the forced nonlinear vibration of the thin cylindrical shell under external excitation, it is necessary to add the external load term to the free vibration displacement equation. The external excitation p is the circumferential cosine distribution simple harmonic load.

$$p(x,\theta,t) = F_x \cos(n\theta)\delta(x)\exp\left[i\left(\frac{\lambda}{R}x - \omega t\right)\right] \tag{5}$$

where F_x represents the circumferential cosine distribution harmonic load amplitude, $\delta(x)$ represents the Dirac function. The positive and negative relationship between the axial wavenumber and the time factor is changed to perform Fourier transformation on the radial, circumferential, axial displacement w, v, u, and excitation p. Convert it to matrix form [17]:

$$\left[N_{3\times3}\right]\left[\tilde{U}_{ns} \quad \tilde{V}_{ns} \quad \tilde{W}_{ns}\right]^T = \left[0 \quad 0 \quad \Omega^2 F_x / \rho h\omega^2\right]^T \tag{6}$$

The coefficient matrix $\left[N_{3\times3}\right]$ is expressed in Appendix A, where the coefficient matrix does not have symmetry. $\Omega = \omega R\sqrt{\frac{\rho(1-\mu^2)}{E}}$ is the dimensionless frequency. The spatial displacement characteristics of thin cylindrical shell are obtained by inverse Fourier transform [29].

$$\begin{bmatrix} u(x) \\ v(x) \\ w(x) \end{bmatrix} = \frac{\Omega^2 F_x}{2\pi\rho h R\omega^2}\begin{bmatrix} \int_{-\infty}^{\infty} M_{13}\exp\left(i\frac{\lambda}{R}x\right)d\lambda \\ \int_{-\infty}^{\infty} M_{23}\exp\left(i\frac{\lambda}{R}x\right)d\lambda \\ \int_{-\infty}^{\infty} M_{33}\exp\left(i\frac{\lambda}{R}x\right)d\lambda \end{bmatrix} \tag{7}$$

where $\lambda = k_{ns}R$ is the dimensionless axial eigenvalues, $M_{3\times3}$ is the inverse matrix of $N_{3\times3}$. By calculating the singular point of the integral function, the integral problem in the infinite domain is transformed into the problem of finding characteristic roots by using the residue theorem. When the dimensionless frequency Ω is known, the dispersion characteristics of the thin cylindrical shell can be obtained from the 8th-degree algebraic equation of dimensionless axial eigenvalue λ under the corresponding boundary conditions.

$$a_8\lambda^8 + a_6\lambda^6 + a_4\lambda^4 + a_2\lambda^2 + a_0 = 0 \tag{8}$$

where $a_i\left(i = 0,2,4,6,8\right)$ is the coefficient of the algebraic equation, which is described in Appendix B. The four pairs of roots of these equations are singular points in the residue theorem, in which real roots, pure imaginary roots, and complex roots correspond to three kinds of vibrating waves with different properties: propagating waves, near-field waves, and attenuating standing waves. According to the basic properties of three kinds of vibration wave propagation, the generation and propagation mechanism of vibration response of the thin cylindrical shell are given, and the analytical solution of the nonlinear displacement response of forced

vibration is obtained.

$$\begin{bmatrix} u(x) \\ v(x) \\ w(x) \end{bmatrix} = \frac{\Omega^2 F_x}{2\pi\rho h R\omega^2} \begin{bmatrix} 2\pi i \sum_{k=1}^{m} Res[M_{13}(\lambda_k)] + \pi i \sum_{k=1}^{8-2m} Res[M_{13}(\lambda_k)] \\ 2\pi i \sum_{k=1}^{m} Res[M_{23}(\lambda_k)] + \pi i \sum_{k=1}^{8-2m} Res[M_{23}(\lambda_k)] \\ 2\pi i \sum_{k=1}^{m} Res[M_{33}(\lambda_k)] + \pi i \sum_{k=1}^{8-2m} Res[M_{33}(\lambda_k)] \end{bmatrix} \tag{9}$$

where m is the number of the conjugate complex roots and pure imaginary roots, 8-$2m$ is the number of real roots and $Res[M_{ij}(\lambda_k)]$ represents the residue of the integrand. The specific expression of the analytical solution of the nonlinear displacement response of forced vibration is expressed in Appendix C.

2.2 Accurate characterization of the straight crack model

Rapid external impact and excessive bending of the thin cylindrical shell are more likely to produce the straight crack. Therefore, it is necessary to derive the local flexibility matrix of the straight crack from the perspective of fracture mechanics, construct the continuous coordination conditions on both sides of the straight crack by LSM, and propose the analytical approach for the nonlinear vibration response of the thin cylindrical shell with a straight crack. Assuming that the shell contains a straight crack with a depth l_0, as shown in Fig. 2. The vertical direction is defined as $\theta = 0^\circ$, the circumferential position of the crack is θ_c, and the relative crack depth is $\xi = l_0 / h$. The relative position of a straight crack on the shell is defined as $\beta = a / L$.

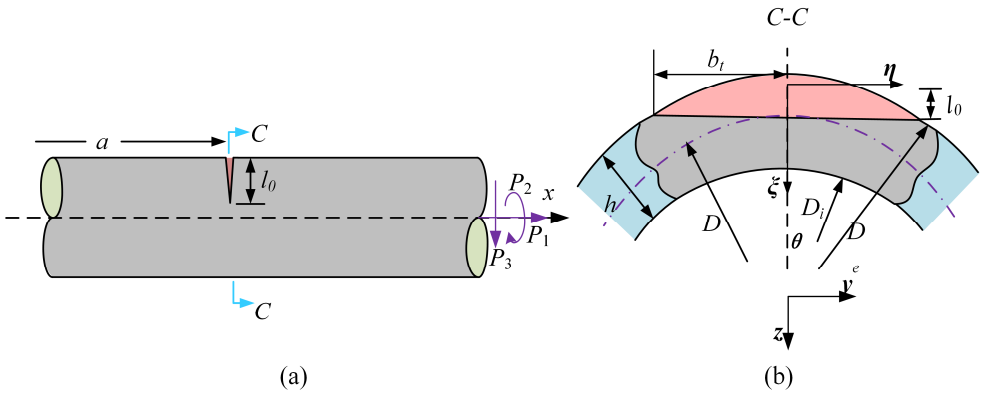

Fig. 2. Thin cylindrical shell with a straight crack. (a) cracked shell, (b) cracked section.

As the research object is a thin cylindrical shell with a straight crack that is not penetrated, the depth and length of a straight crack are minimal. Therefore, the wave superposition principle can be used to solve the displacement response of the thin cylindrical shell with a straight crack, that is, the superposition of the vibration waves caused by the circular crack and the vibration waves of the ideal thin cylindrical shell.

The external excitation can make the thin cylindrical shell generate four vibration waves. Each wave can transmit and reflect when these vibration waves are transmitted to the crack region, resulting in the generation of four transmission waves and reflected waves. Assuming that the external excitation position is $x=b\left(0<b<a\right)$, four incident waves (similar to the ideal thin cylindrical shell) exist in the axial range of $0\le x\le b$, four incident waves and reflected waves caused by the straight crack exist in the axial range of $b\le x\le a$, and four transmission waves caused by the straight crack exist in the axial range of $a\le x\le L$. Their interaction affects the nonlinear displacement response, and the radial displacement of a particular circumferential mode *n* can be expressed as.

$$\begin{cases} w_a = W_a\left(x\right)\cos\left(n\theta\right)=\sum_{s=1}^{4}W_{ns}\exp\left(ik_{ns}\left(x-b\right)+i\omega t\right)\cos\left(n\theta\right) & 0\le x\le b \\ w_b = W_b\left(x\right)\cos\left(n\theta\right)=\sum_{s=1}^{4}W_{n(s+4)}\exp\left(-ik_{ns}\left(x-b\right)+i\omega t\right)\cos\left(n\theta\right)+ & \\ \qquad \sum_{s=1}^{4}W_{n(s+8)}\exp\left(ik_{ns}\left(x-a+b\right)+i\omega t\right)\cos\left(n\theta\right) & b\le x\le a \\ w_c = W_c\left(x\right)\cos\left(n\theta\right)=\sum_{s=1}^{4}W_{n(s+12)}\exp\left(ik_{ns}\left(x-a+b\right)+i\omega t\right)\cos\left(n\theta\right) & a\le x\le L \end{cases} \tag{10}$$

where $W_a\left(x\right)$, $W_b\left(x\right)$ and $W_c\left(x\right)$ are the radial displacement amplitude of each region, and $W_{ns}\left(s=1\sim16\right)$ is the wave amplitude. As long as these unknown parameters are known, the radial displacements of each point can be obtained. The existence of cracks does not cause the phase change of reflected wave, transmitted wave and vibration wave of the ideal thin cylindrical shell [29]. Therefore, combined with the radial displacement amplitude $w\left(x\right)$ of the ideal shell, the displacement amplitude w_r on the thin cylindrical shell with a straight crack can be obtained through the wave superposition principle, which is expressed as

$$w_r=\left(W_i\left(x\right)-w\left(x\right)\right)\cos\left(n\left(\theta-\theta_c\right)\right)+w\left(x\right) \tag{11}$$

where $W_i\left(x\right)\left(i=a,b,c\right)$ represents the radial displacement amplitude. Using the same method, the axial and circumferential displacements can also be expressed as

$$u_r=\left(U\left(x\right)-u\left(x\right)\right)\cos\left(n\left(\theta-\theta_c\right)\right)+u\left(x\right) \tag{12}$$

$$v_r=\left(V_c\left(x\right)-v\left(x\right)\right)\sin\left(n\left(\theta-\theta_c\right)\right)+v\left(x\right) \tag{13}$$

When the circumferential position of the straight crack is $\theta=\theta_c$, according to the LSM [30], it can be known that the straight crack can produce additional local flexibility, causing discontinuities in the stress and displacement on both sides of the straight crack. The LSM can describe discontinuity.

$$\Delta_i^+-\Delta_i^-=C_{ij}P_i \tag{14}$$

where Δ_i^+ and Δ_i^- represent the generalized displacement on both sides of the straight crack, C_{ij} represents local flexibility, and P_i represents generalized internal force.

The SIFs cannot be obtained directly for straight crack. Due to the cross-section of the straight crack being arc-shaped, the arc-shaped area needs to be discretized into countless rectangular areas. The additional strain energy of the rectangular area is calculated to obtain the local flexibility coefficient of the straight crack. According to the basic theory of local flexibility, the additional strain energy caused by the straight crack can be expressed [31].

$$U_T = \int_{A_c} J dA = \int_0^{l_0} \int_{-b_t}^{b_t} J d\eta d\xi' \tag{15}$$

where A_c is the effective area of crack area, J is the additional strain energy release rate caused by the straight crack, b_t is the half of straight crack width, ξ' is the local depth variable, and η is the offset variable in the tangential direction of the crack top. When the boundary condition of the thin cylindrical shell is clamped-clamped, the local flexibility of the straight crack is mainly affected by the mode *I* (opening mode) crack and mode *II* (sliding mode) crack, thus the mode *III* (tearing mode) crack is no longer considered. The additional strain energy release rate caused by the straight crack can be described.

$$J = \frac{1}{E'}\left[\left(K_{I1} + K_{I2} + K_{I3}\right)^2 + K_{II2}^2\right] \tag{16}$$

where K_{I1}, K_{I2} and K_{I3} represent the SIFs of the mode *I* (opening mode) crack caused by the axial force, shear force, and bending moment, and K_{II2} represents the SIFs of the mode *II* (sliding mode) crack caused by the shear force. When it is in a plane strain state, $E' = \dfrac{E}{1-\mu^2}$, and when it is in a plane stress state, $E' = E$.

According to the Castigliano theorem, the additional nonlinear displacement induced by the straight crack can be expressed by the derivative of the strain energy with respect to the force.

$$U_i = \partial U_T / \partial P_i = \frac{\partial}{\partial P_i} \int_0^{l_0} \int_{-b_t}^{b_t} J d\eta d\xi' \tag{17}$$

Therefore, the additional local flexibility matrix can be expressed as [30]:

$$C_{ij} = \partial U_i / \partial P_j = \frac{\partial}{\partial P_i P_j} \int_0^{l_0} \int_{-b_t}^{b_t} J d\eta d\xi' \tag{18}$$

Based on the local flexibility matrix, the displacement coordination condition on both sides of the straight crack can be obtained:

$$\left[u^+ - u^- \quad \frac{\partial w^+}{\partial x} - \frac{\partial w^-}{\partial x} \quad w^+ - w^- \quad v^+ - v^-\right]^T = \left[C_{4\times4}\right]\left[N_x \quad M_x \quad Q_x \quad T_{x\theta}\right]^T \tag{19}$$

where the superscript symbols + and − of the displacements in each direction represent the right and left sides of the crack section, respectively, and Q_x is the

radial shear force. Therefore, the four displacement coordination equations on both sides of the crack can be acquired. Then, eight displacement and stress conditions at the external excitation and four stress conditions at the crack are listed, as shown in Eqs. (20-22). Therefore, each unknown wave amplitude of Eq. (10) can be acquired.

$$N_x^R = N_x^L, M_x^R = M_x^L, Q_x^R = Q_x^L, N_{x\theta}^R = N_{x\theta}^L \qquad (x=a) \tag{20}$$

$$u^R = u^L, \partial w^R / \partial x = \partial w^L / \partial x, w^R = w^L, v^R = v^L \qquad (x=b) \tag{21}$$

$$N_x^R = N_x^L, M_x^R = M_x^L, T_{x\theta}^R = T_{x\theta}^L, S_x^R = S_x^L + F \qquad (x=b) \tag{22}$$

The solution of local flexibility has become the most key factor. To simplify the calculational difficulty, for the depth l_0 of the straight crack, the $\xi' - \eta$ coordinate system is transformed into the *y*-*z* coordinate system, as shown in Fig. 2(b). Assuming $z = \xi / D_e$ and $y = \eta / D_e$, the $d\xi' = D_e dz$, $d\eta = D_e dy$ are obtained.

The thin cylindrical shell with a straight crack is subjected to the combined action of axial force P_1, bending moment P_2, and shear force P_3. The local flexibility matrix of the straight crack area is

$$C_{11} = \frac{32}{\pi(1-\gamma^2)^2 E' D_e} \int_0^{a/D_e} \int_{-\sqrt{1-z^2}}^{\sqrt{1-z^2}} \beta F_1^2(s) dy dz \tag{23}$$

$$C_{12} = \frac{256 L_c}{\pi(1-\gamma^2)(1-\gamma^4) E' D_e^2} \int_0^{a/D_e} \int_{-\sqrt{1-z^2}}^{\sqrt{1-z^2}} \alpha^{0.5} \beta F_1(s) F_2(s) dy dz \tag{24}$$

$$C_{13} = \frac{256}{\pi(1-\gamma^2)(1-\gamma^4) E' D_e^2} \int_0^{a/D_e} \int_{-\sqrt{1-z^2}}^{\sqrt{1-z^2}} \alpha^{0.5} \beta F_1(s) F_2(s) dy dz \tag{25}$$

$$\begin{aligned} C_{22} = {} & \frac{32}{\pi(1-\gamma^2)^2 E' D_e} \int_0^{a/D_e} \int_{-\sqrt{1-z^2}}^{\sqrt{1-z^2}} \beta F_{II}^2(s) dy dz \\ & + \frac{2048 L_c^2}{\pi(1-\gamma^4)^2 E' D_e^3} \int_0^{a/D_e} \int_{-\sqrt{1-z^2}}^{\sqrt{1-z^2}} \alpha\beta F_2^2(s) dy dz \end{aligned} \tag{26}$$

$$C_{23} = \frac{2048 L_c}{\pi(1-\gamma^4)^2 E' D_e^2} \int_0^{a/D_e} \int_{-\sqrt{1-z^2}}^{\sqrt{1-z^2}} \alpha\beta F_2^2(s) dy dz \tag{27}$$

$$C_{33} = \frac{2048 L_c}{\pi(1-\gamma^4)^2 E' D_e^3} \int_0^{a/D_e} \int_{-\sqrt{1-z^2}}^{\sqrt{1-z^2}} \alpha\beta F_2^2(s) dy dz \tag{28}$$

$$C_{21}=C_{12} \quad C_{31}=C_{13} \quad C_{32}=C_{23} \quad C_{41}=C_{42}=C_{43}=C_{44}=0 \tag{29}$$

where $\alpha = 1-4y^2$, $\beta = z + \sqrt{1/4 - y^2}$, the correction factor of stress intensity F_1, F_2 and F_{II} are described by [32]:

$$F_1(s) = F_4(s)\left(0.751 + 2.02s + 0.37(1-\sin\lambda)^3 / \cos\lambda\right) \tag{30}$$

$$F_2(s) = F_4(s)\left(0.923 + 0.199(1-\sin\lambda)^4 / \cos\lambda\right) \tag{31}$$

$$F_{II}(s) = \left(1.122 - 0.561s + 0.085s^2 + 0.18s^3\right) / \sqrt{1-s} \tag{32}$$

$$F_4(s) = \sqrt{\tan\lambda / \lambda} \tag{33}$$

where the coefficients can be solved by $\lambda = \frac{\pi s}{2}$, $s = \frac{2z + \sqrt{1-4y^2}}{2\sqrt{1-4y^2}}$.

Substitute the result of these Eqs. (23-29) into Eq. (14), and combine it with Eqs. (20-22) to obtain the displacement response amplitude of the thin cylindrical shell with a straight crack, which can directly reflect the circumferential position of the straight crack.

The additional local flexibility matrix calculation reflects the local mechanical behavior at the straight crack. And the key factor in obtaining the free vibration characteristics of the thin cylindrical shell with a straight crack is to solve the stiffness matrix of the cracked shell element. The totality flexibility of a straight cracked shell can be equivalent to the algebraic sum of the flexibility of the thin cylindrical shell and the additional flexibility caused by a straight crack [33], which can be solved by

$$\begin{aligned} \boldsymbol{C}_{tot} &= \boldsymbol{C}_{nocrack} + \boldsymbol{C}_{crack} \\ &= \begin{bmatrix} \dfrac{L}{EA} + c_{11} & -c_{12} & -c_{13} \\ -c_{21} & \dfrac{L^3}{3EI} + c_{22} & \dfrac{L^2}{2EI} + c_{23} \\ -c_{31} & \dfrac{L^2}{2EI} + c_{32} & \dfrac{L}{EI} + c_{33} \end{bmatrix} \end{aligned} \tag{34}$$

where I is the second moment of area, and A is the sectional area. The stiffness matrix of the thin cylindrical shell with a straight crack can be described as

$$\boldsymbol{K}_e = \boldsymbol{T}\boldsymbol{C}_{tot}^{-1}\boldsymbol{T}^T \tag{35}$$

where the transformation matrix $\boldsymbol{T}$ is shown in

$$\boldsymbol{T} = \begin{bmatrix} -1 & 0 & 0 & 1 & 0 & 0 \\ 0 & -1 & -L_e & 0 & 1 & 0 \\ 0 & 0 & -1 & 0 & 0 & 1 \end{bmatrix}^T \tag{36}$$

The thin cylindrical shell can be regarded as a dynamic system composed of mass, damping, and stiffness matrix. When crack damage occurs in the thin cylindrical shell, the basic parameters of the thin cylindrical shell change accordingly, resulting in the change of modal vibration parameters (such as natural frequency, damping, and mode).

Assuming that the straight crack does not change the mass matrix of the structure and ignoring the damping effect of the thin cylindrical shell, the characteristic equation of free vibration of the thin cylindrical shell with a straight crack can be expressed as [34]

$$\left(\boldsymbol{K}_e - \omega^2 \boldsymbol{M}\right)\boldsymbol{\Phi} = 0 \tag{37}$$

where $\boldsymbol{M}$ represents the mass matrix of the thin cylindrical shell, ω and $\boldsymbol{\Phi}$ represent the natural circular frequencies and vibration modes of the thin cylindrical shell with a straight crack, respectively. The natural frequency and vibration mode of the thin cylindrical shell with a straight crack can be obtained by eigenvalue analysis.

2.3 Straight crack identification method

There is a direct correlation between the nonlinear vibration response of the thin cylindrical shell and the straight crack morphology. For the clamped-clamped boundary condition, the natural frequency only depends on the relative depth and position of the straight crack. And the straight crack changes the local flexibility coefficient of the thin cylindrical shell and the nonlinear displacement response characteristics of each point in the circumferential direction. According to the nonlinear vibration response characteristics of the thin cylindrical shell with a straight crack, the straight crack identification method based on the natural frequency isolines [35] and amplitude maximization methods is proposed. The flow chart of quantitative diagnosis of the straight crack in the thin cylindrical shell is as follows.

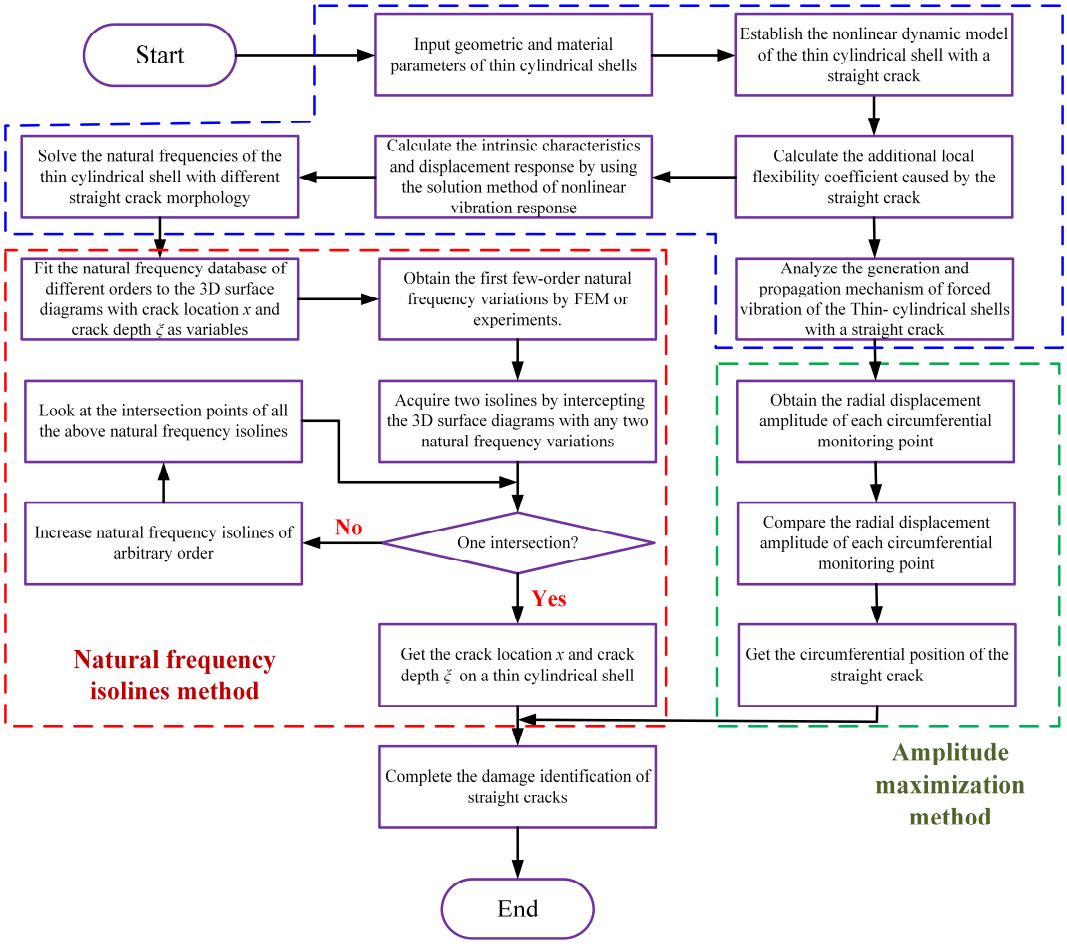

Fig. 3. The flow diagram of the straight crack fault diagnosis

According to the analytical approach for nonlinear vibration response of the thin cylindrical shell with a straight crack, the natural frequency database under different straight crack morphology is established. The natural frequency variations of different orders can be obtained by FEM or experimental test, and then the natural frequency isolines map at different relative depths and locations can be drawn. Since the straight crack point appears on different natural frequency isolines, there

must be an intersection point between the two isolines. If the intersection point is not unique, another isoline of a different order can be added. The intersection point represents the relative depth and position information of the straight crack. The straight crack changes the displacement response characteristics of each point in the circumferential direction. The circumferential information of a straight crack is obtained by analyzing the radial displacements at different circumferential positions.

3 Numerical verification

Based on the local flexibility theory and wave superposition principle, the new analytical approach for nonlinear vibration response of the thin cylindrical shell with a straight crack is proposed to reveal the evolution law of nonlinear vibration response. And combined with natural frequency isolines and amplitude maximization methods, the nonlinear vibration signal identification method for straight crack damage is developed. Due to the lack of previous studies in the field discussed in this study, no similar literature could provide data to verify the effectiveness and accuracy of the proposed analytical method. Therefore, it is necessary to ensure the correctness of the most critical factors (local flexibility coefficient and shell theory) in the solution process and establish the FEM to verify the accuracy of the final analytical results. Firstly, the local flexibility coefficient solution of the straight crack under pure bending moment is compared with the experimental results [21]. Then, the FEM of the thin cylindrical shell is established according to the material properties and dimensions of the literature, and its modal analysis should be carried out. The analytical, literature [36] and FEM results are compared and verify the reliability of the shell model adopted. Finally, the FEM of the thin cylindrical shell with a straight crack is established, and the analytical results of displacement response amplitude of circumferential monitoring points and natural frequency with different crack depths are compared with the FEM results for evaluation, which verifies the accuracy of the analytical method for nonlinear vibration response of the thin cylindrical shell with a straight crack. The straight crack identification method can be validated using a numerical case in section 4.4.

3.1 Verification of local flexibility coefficient

From Eq. (14), it can be found that the local flexibility coefficient is the key factor in solving nonlinear vibration responses and natural modes. According to the theory of linear fracture mechanics, the dimensionless flexibility of the thin cylindrical shell with a straight crack under axial force, shear force, and bending moment can be obtained. Naniwadekar experimentally measured the local flexibility of the thin cylindrical shell under the action of the pure bending moment [21], and obtained the torsional spring stiffness of the thin cylindrical shell with different crack depths

under the action of the pure bending moment, which can be converted into local flexibility coefficient. Based on the properties (L=0.95m, R=0.0328m, h=0.01m, E=173.81GPa, ρ=7860kg/m^3, μ=0.3) of the thin cylindrical shell described in the literature [21], the analytical solution of the local flexibility coefficient of the benchmark model is obtained by using the solution method of the local flexibility coefficient. The diagram between the analytical and reference results of the local flexibility coefficient of the straight crack is shown in Fig. 4.

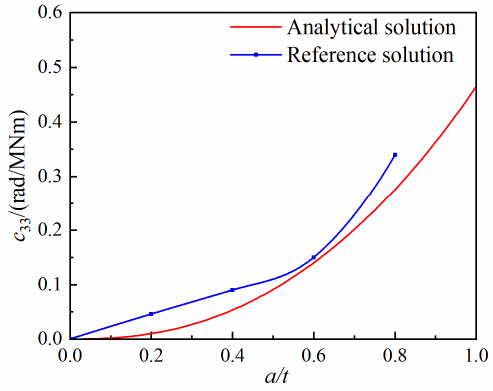

Fig. 4. The analytical and reference results of the local flexibility coefficient of the straight crack.

It can be found that the analytical solution of the local flexibility coefficient is basically consistent with the reference results, and the local flexibility coefficient can grow exponentially with the increase of the straight crack depth. However, the analytical results are still slightly lower than the reference results, and the reason for this phenomenon is related to the form of straight crack generation in the experiment. The prespecified crack in the experiment is a straight crack with a thickness of 0.2mm generated by the line cutting, which could not imitate the breathing crack entirely, increasing the local flexibility coefficient of the straight crack [21]. Therefore, the theoretical derivation and analytical method for the local flexibility coefficient of the thin cylindrical shell with a straight crack can effectively reflect the variation of the local flexibility coefficient caused by the straight crack, which has strong credibility and can accurately obtain the natural frequency and nonlinear displacement response.

3.2 Validation of nonlinear vibration response

The natural frequency and nonlinear displacement responses of the thin cylindrical shell with a straight crack are hardly reported in the existing literature. In this case, the three-dimensional FEM of the thin cylindrical shell with a straight crack is one of the most appropriate procedures for investigating the accuracy of the proposed analytical method of the nonlinear vibration response. Based on the properties and dimensions (L/R=20, h/R=0.01, R=1m, μ=0.3, ρ=7850kg/m^3, E=210GPa) in the literature [36], the FEM is simplified into an ideal thin cylindrical shell, and the boundary conditions are set as clamped-clamped, the modal analysis

of the thin cylindrical shell is carried out, and the corresponding analytical values are calculated. The first eighth natural frequency, corresponding analytical results, and reference results are extracted, as shown in Table 1. The maximum error between the natural frequency of the analytical and the FEM results is less than 1.3%, which verifies the correctness of the adopted shell model and the proposed natural frequency solution method.

Table. 1. Comparison of the natural frequency of the thin cylindrical shell with a clamped-clamped boundary condition.

Order	Analytical	Reference [36]	FEM	Error (%)	Mode (s,n)
1	12.13	12.17	12.25	-0.97	(1,2)
2	19.61	19.61	19.64	-0.15	(1,3)
3	23.28	23.28	23.18	+0.43	(2,3)
4	28.06	28.06	27.69	+1.29	(2,2)
5	31.97	31.98	31.60	+1.17	(3,3)
6	36.48	36.47	36.70	-0.60	(1,4)
7	37.38	37.37	37.55	-0.45	(2,4)
8	39.77	39.78	39.87	-0.25	(3,4)

The critical factors in the solution process have been verified above, but the final analytical results of the nonlinear vibration response of the thin cylindrical shell with a straight crack have not been verified. To improve the applicability of the thin cylindrical shell, the parameters of the analytical model and FEM are set as follows: L/R=40, h/R=0.1, R=0.1m, μ=0.3, ρ=7850kg/m^3, E=210GPa. The axial position of the straight crack is set as x=2.0m, the circumferential position is set as $\theta_c = 0$, and the boundary conditions are set as clamped-clamped. In the process of establishing the FEM of the thin cylindrical shell with a straight crack, it is very challenging to formulate an appropriate meshing strategy. Considering the influence of the crack tip mesh on the FEM results, the crack tip is locally encrypted. A gradient layer is added around the crack tip to transfer data into a structured grid of other domains efficiently. To select the most appropriate mesh configuration, it is necessary to compare the FEM results of the first-order natural frequencies under different mesh numbers to verify mesh independence, as shown in Fig. 5(a). As the number of meshes increases, the first-order natural frequency can converge gradually. For the mesh configuration with more than 77201 meshes, the natural frequencies are basically unchanged and agree with the analytical solution. Therefore, the meshes number 77201 is applied to solve the forced nonlinear vibration response of the thin cylindrical shell with a straight crack. The external excitation position is x=1.0m, the external excitation is circumferential cosine distribution simple harmonic load with the frequency of 100Hz and amplitude of 100N, and the monitoring position is x=3.0m (same as in Section 4.2). A comparison of radial displacement amplitudes of circumferential monitoring points

with different crack depths is shown in Fig. 5(b). The green shaded area represents a 3% error band based on the FEM results. The analytical solution is entirely within the range of the error band, which can fully prove the correctness and accuracy of the analytical approach for the nonlinear vibration response of the thin cylindrical shell with a straight crack.

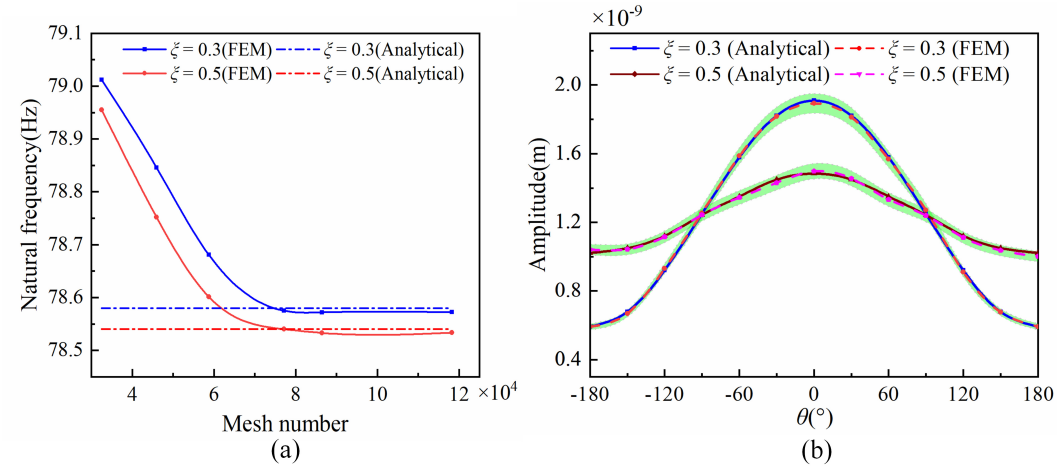

Fig. 5. Nonlinear vibration response verification of the thin cylindrical shell with different crack depths. (a) Natural frequencies under different mesh numbers, (b) Radial displacement amplitudes of circumferential monitoring points.

4 Results and discussions

Utilizing the analytical approach for the nonlinear vibration response of the thin cylindrical shell with a straight crack, we need to complete the following four objectives to analyze the nonlinear vibration response characteristics: *i*) determine the corresponding relationship and transformation law between the straight crack morphology and the natural frequency; *ii*) explore the generation and propagation mechanism of forced nonlinear vibration response; *iii*) obtain the nonlinear displacement response characteristics of the thin cylindrical shell with a straight crack and reveal the displacement evolution law of different directions; *iv*) find a nonlinear vibration signal identification method for straight cracks and verify the proposed identification method by a numerical example.

4.1 Natural frequency transformation characteristics

Due to the first few natural frequencies of the thin cylindrical shell being convenient and accurate, the first three-modes should be used as the input parameters for straight crack identification. Since the relative length of the research object is L/R=40, the shell belongs to the medium-long shell. Thus, the axial mode dominates the low-order modes, and the first three-modes are (0,1), (0,2), and (0,3). The other parameters are set as h/R=0.1, R=0.1m, μ =0.3, ρ =7850kg/m^3, E=210GPa. Due to the thickness being relatively thin, the lower natural frequency

does not change much. To better explore the transformation relationship between the straight crack morphology and the natural frequency, the difference in the low-order natural frequency between the cracked thin cylindrical shell and the ideal shell is defined as $f^{'} = f_c - f$.

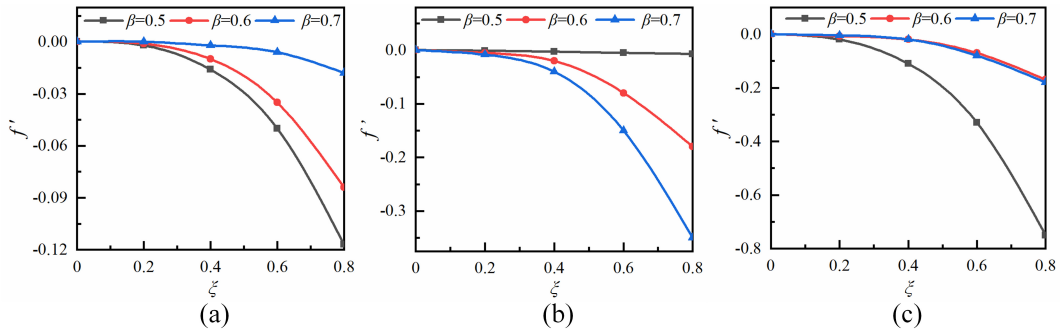

Fig. 6. Natural frequency transformation characteristics of the different relative crack depths. (a) first-order, (b) second-order, (c) third-order.

Due to the marvelous symmetry of the thin cylindrical shell with clamped-clamped boundary conditions, the straight crack positions are set in the right half of the shell: β=0.5, 0.6, 0.7. Keeping the straight crack position unchanged, the relationship curves between the first three natural frequencies and the relative depth of the straight crack are shown in Fig. 6. It can be seen that the natural frequency variation curves are all below the zero-axes, indicating that the existence of straight crack reduces the shell stiffness and decreases the natural frequency. When the crack location is determined, the natural frequencies of each order decrease with the increase of crack depth. From the difference in natural frequencies of different orders, it can be seen that the changing trend of the three curves is gradually reversed, which is mainly determined by the position of the straight crack in the mode shape of the thin cylindrical shell. At the same time, the effect of straight crack on higher order natural frequency is greater.

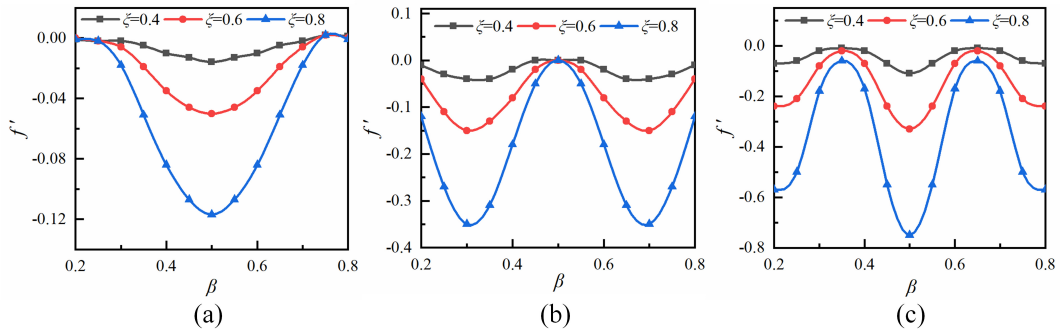

Fig. 7. Natural frequency transformation characteristics of the different crack position. (a) first-order, (b) second-order, (c) third-order.

The relative depths of the straight crack are kept unchanged as ξ=0.4, 0.6, and 0.8, respectively, and the variation curves of the natural frequency with the relative position are shown in Fig. 7. When the straight crack is located in the middle section,

as shown in Fig. 7(a), the first-order natural frequency decreases most rapidly. As the straight crack moves to both ends, the influence of the relative crack position on the first-order natural frequency becomes less and less, showing a quadratic function curve. In Fig. 7(b), the middle position is a node of the second-order, and the variation of the second-order natural frequency with different crack depths is zero. The minimum values are on both sides of the middle section, where the second-order natural frequency is the most sensitive to the straight crack. As shown in Fig. 7(c), there are two nodes in the third-order natural frequency variation curve. Similarly, there is a minimum in the middle of two adjacent nodes. Therefore, it can be seen that when the straight crack is located near odd times of $L/2n$, the nth order natural frequency difference of the thin cylindrical shell has a minimum, and when the crack is located near even times of $L/2n$, the nth order natural frequency difference has a maximum, which is very close to zero. This phenomenon indicates that the natural frequency is very insensitive to the straight crack when the crack is located at the node of a certain mode.

4.2 Generation and propagation mechanism of nonlinear vibration

The thin cylindrical shell in engineering production and daily application is often subject to various external nonlinear excitations, and the corresponding nonlinear vibration responses are determined by their structure, component parameters, and boundary conditions. The vibration generation and propagation mechanism of the forced thin cylindrical shell are studied to obtain the displacement response characteristics of the forced vibration, which can provide an intuitive and accurate data basis for the state detection of the thin cylindrical shell.

The essential parameters are shown in Section 4.1. To simulate the vibration caused by external factors, the circumferential cosine distribution simple harmonic load with amplitude of $F_x = 100N/m$ is applied at x=1.0m. When the circumferential mode number is n=0, the characteristic roots are shown in Table 2. According to the characteristic root, the basic type of wave can be determined. To analyze the displacement amplitude response, only the range of 1.0≤x≤3.0m in the right half is discussed here.

It can be found from Table 2 that the characteristic equation contains the real root and complex roots (or pure imaginary root), so the displacement response is the result of the joint action of the propagation wave and the attenuated standing wave (or near field wave). From Fig. 8(b), it can be seen that the circumferential displacement response under the circumferential cosine distribution simple harmonic load is not generated; that is, the axial and radial displacement responses are decoupled from each other. Due to the shell vibrating only in the axial and radial directions, the vibration behavior of the shell is similar to the breathing action. Therefore, the vibration mode when the circumferential mode number is zero is also called breathing mode, and the decoupling feature of the breathing mode can

provide ideas for later straight crack identification. When the dimensionless frequency is $\Omega = 0.012998$, it can be seen from Table 2 that the characteristic equation of the shell system contains two pairs of real roots and two pairs of complex roots. In this case, the displacement response is the interaction result between the propagating wave and the attenuated standing wave. In Fig. 8(a), the axial displacement amplitude increases quickly with the axial coordinate first, indicating that the attenuated standing wave is the main component affecting the axial displacement at the initial stage. In the vicinity of x=1.07m, the axial displacement amplitude reaches the maximum value. Then the attenuated standing wave component with high-order exponential term rapidly decays to zero with the increase of axial coordinates. Hence, the change of the displacement amplitude curve tends to be gentle. Meanwhile, the axial displacement is mainly affected by the action of the propagating wave. In Fig. 8(c), the radial displacement amplitude reaches its maximum value at x=1.0m, then rapidly declines, and an inflection point appears near x=1.09m. The curve fluctuates in the form of a string function with an order of 10^{-12} when x>1.23m. At the time, the shell is mainly affected by the propagation wave, and due to the real roots being small, the effect is not apparent. When the dimensionless frequency is $\Omega = 0.5$, the form of the eigenvalues of the shell system characteristic equation is similar to that of the previous case, containing two pairs of real roots and two pairs of complex roots. The thin cylindrical shell is acted by both the propagating wave and the attenuated standing wave, but the value of the real root of the former is larger. When the axial displacement amplitude reaches the maximum value near x=1.06m, it shows an obvious chord function change. And the amplitude fluctuation range is larger than that in the previous case, which indicates that the real roots can significantly increase the acting proportion and acting effect of the propagating wave, thus increasing the vibration displacement response of the shell. Similarly, the variation effect of the radial displacement amplitude is the same as that of the axial displacement amplitude, indicating that with the increase of the dimensionless natural frequency, the action proportion and effect of the propagating wave become larger, and the displacement response amplitude of the thin cylindrical shell increases. When the dimensionless frequency is $\Omega = 1.2$, the eigenvalues of the shell system characteristic equations are transformed into three pairs of real roots and one pair of purely imaginary roots; that is, there are three propagating waves and one near-field wave. Each propagating wave contains elements of stretching, twisting, and bending. It can be seen from Fig. 8 that the axial and radial displacement amplitudes show a sharp increase near the zero axes, mainly because the near-field wave plays a huge role here. Then, the amplitude curves prove the obvious wave superposition effect, which is mainly the result of the joint action of three propagation waves in two directions.

Table. 2. Roots of the characteristic equation. (n=0)

Ω=0.012998	Ω=0.5	Ω=1.2
0.0136	0.5330	1.0923
-0.0136	-0.5330	-1.0923
0.0219	0.8441	2.0258
-0.0219	-0.8441	-2.0258
-4.0848+4.0479i	-3.7718+3.7340i	5.0653
4.0848+4.0479i	3.7718+3.7340i	-5.0653
-4.0848-4.0479i	-3.7718-3.7340i	4.9809i
4.0848-4.0479i	3.7718-3.7340i	-4.9809i

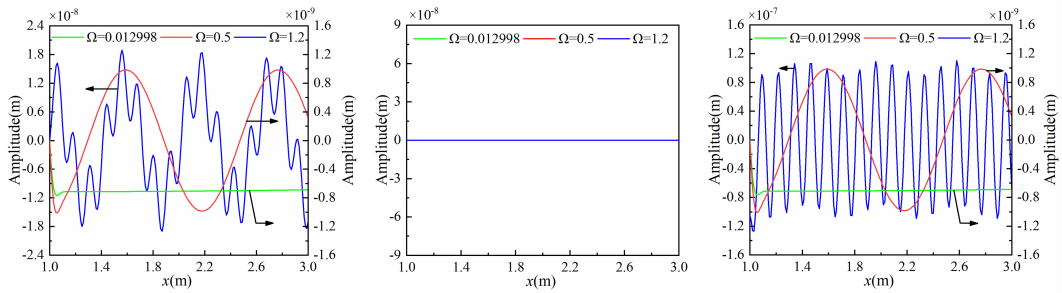

Fig. 8. The displacement amplitude response of the ideal thin cylindrical shell. (n=0) (a) axial direction, (b) circumferential direction, (c) radial direction.

According to the above analysis, the axial and radial displacements in the breathing mode have decoupling characteristics, which can be inferred: the thin cylindrical shell has no circumferential torsion, and the axial and radial displacements at the same axial position are the same everywhere; when the characteristic equation of the shell system contains real roots, as the value of the real roots increases, the acting proportion and effect of corresponding propagating waves also increase significantly, and the oscillation frequency of the displacement amplitude curve increases; when the characteristic equation contains the pure virtual root, and the value is small, the effect of the near-field wave on the displacement response is great, but only in the initial stage. When the number of propagation waves in the thin cylindrical shell is more than one and more waves have similar effects in a certain direction, the displacement amplitude curve appears to be an obvious wave superposition effect.

4.3 Forced nonlinear vibration response

Through the above analysis shows that under the breath mode(n=0), the axial and radial displacement of the thin cylindrical shells mutual decouple. Therefore, the displacement amplitude of the circumferential points in the arbitrary axial direction should be equal when a cosine distribution simple harmonic load is applied to the

circumferential direction. When there is a straight crack in the thin cylindrical shell, the additional local flexibility in the straight crack region makes the propagation of vibration waves in the shell bound to change. So the displacement response of circumferential points does not have equality, which provides a new idea for straight crack identification.

To simplify the analysis, the axial position of the straight crack is set as x=2.0m, and the circumferential position is set as $\theta_c = 0$. According to Eqs. (11-13), it can be found that the displacement amplitude of the thin cylindrical shell with a straight crack is highly symmetric, so only the half-cycle shell is analyzed. Seven circumferential monitoring points are set at x=2.2m, 2.4m, 2.6m, 2.8m, 3.0m, and 3.2m in the right half of the shell, respectively. The circumferential positions are 0°, 30°, 60°, 90°, 120°, 150° and 180°. The monitoring points are numbered alphabetically along the axis and are denoted as A, B, C, D, E, and F from near to far. Similarly, the circumferential positions of the monitoring points are numbered, and the phases from small to large are 0, 1, 2, 3, 4, 5, and 6. Therefore, the circumferential monitoring points at x=3.0m can be expressed as: $E_0, E_1, E_2, E_3, E_4, E_5$ and E_6. The angle difference between the monitoring point and the circumferential position of the straight crack is defined as $\theta_d = |\theta - \theta_c|$.

The circumferential cosine distribution simple harmonic load is the same as in Section 4.2. The axial, circumferential, and radial displacement responses of each monitoring point of the ideal thin cylindrical shells in the axial position E are shown in Fig. 9. The whole system tends to be stable, the axial and radial displacement responses all show the normal chord function fluctuation, and the curves of each monitoring point completely coincide. The circumferential displacement response is almost zero, indicating that the ideal thin cylindrical shell is decoupled from the axial and radial displacement under the circumferential cosine distribution simple harmonic load, which is consistent with the previous analysis.

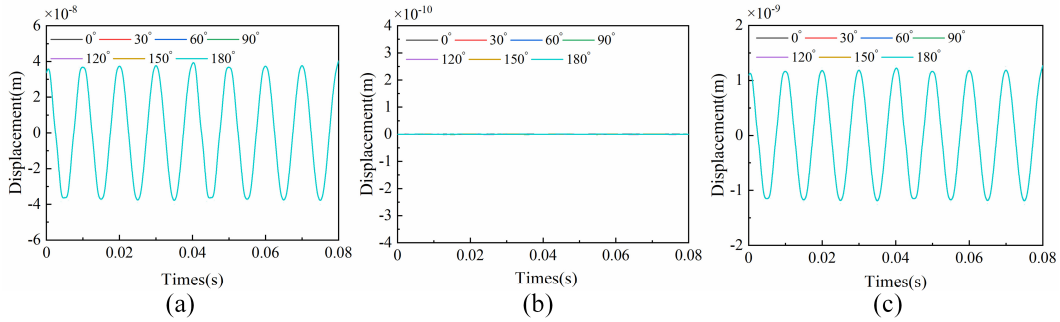

Fig. 9. Displacement response of the circumferential monitoring points at E (ξ=0). (a) axial direction, (b) circumferential direction, (c) radial direction.

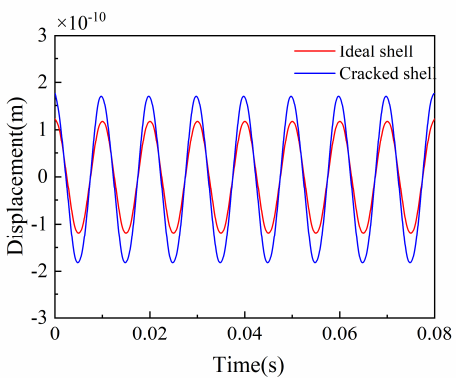

Fig. 10. Comparison of radial displacement responses of cracked shells and ideal shells at E_0.

Setting the relative crack depth ξ=0.5, the nonlinear vibration response of the thin cylindrical shell with a straight crack is analyzed. The radial displacement response of the monitors at E_0 is extracted and compared with that of the ideal shells, as shown in Fig. 10. The displacement response amplitude of the monitoring point E_0 at the thin cylindrical shell with a straight crack is significantly larger than that of the ideal shell, and the phase of the two peaks is consistent. The reason for this phenomenon is that the existence of straight cracks affects the path of vibration wave propagation and local flexibility inside the shell. When the vibration wave propagates to the straight crack, the reflected wave and transmitted wave can be generated. Although the energy of the transmitted wave is weakened relative to the vibration wave, the reduction of local flexibility leads to a small increase in the displacement response. The axial, circumferential, and radial displacement responses of circumferential monitoring points at *E* are extracted as shown in Fig. 11. In Fig. 11(a), the axial displacement response curves of circumferential monitoring points are almost identical to those without straight crack. However, there is an apparent circumferential displacement response at *E* in Fig. 11(b). With the increase of the phase angle, the circumferential displacement amplitude first increases and then decreases, indicating that the existence of the straight crack destroys the decoupling characteristics of circumferential and radial direction. As shown in Fig 11(c), the radial displacement response of each monitoring point showed a significant decreasing trend with the increase of the phase angle. The circumferential angle of the point E_0 is consistent with that of the straight crack, and the displacement amplitude is the largest. On the contrary, The circumferential angle difference between the point E_6 and the straight crack is the largest, and the radial displacement amplitude was the smallest, indicating a certain correspondence between the radial displacement amplitude of the circumferential points the circumferential position of the straight crack.

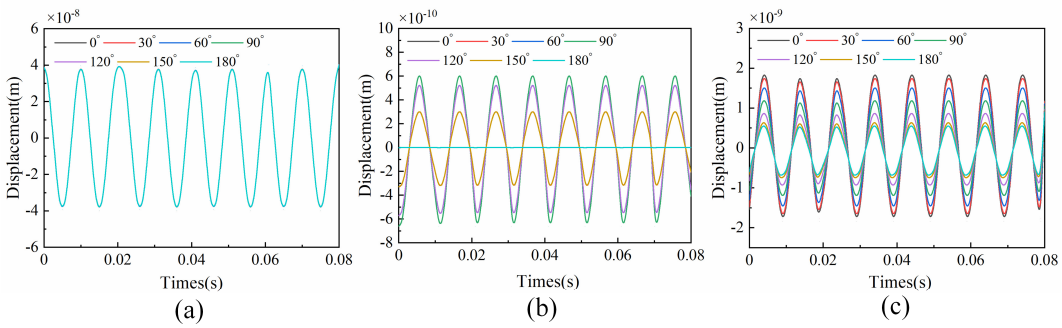

Fig. 11. Displacement response of the circumferential monitoring points at E (ξ=0.5). (a) axial direction, (b) circumferential direction, (c) radial direction.

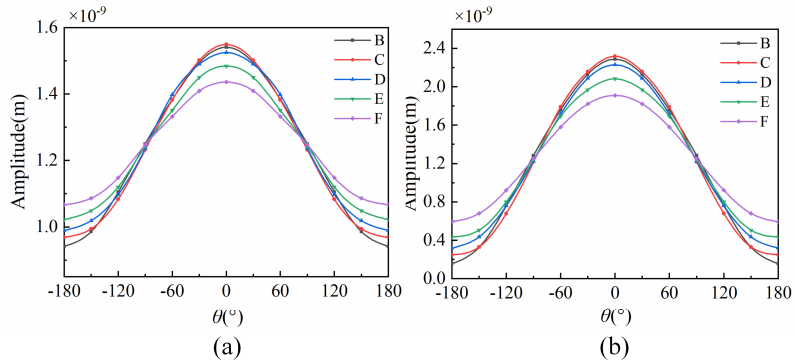

Fig. 12. Radial displacement amplitude of the circumferential monitoring points at each axial position. (a) ξ=0.3 , (b) ξ=0.5 .

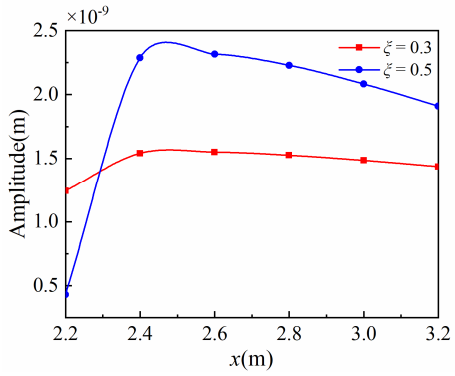

Fig. 13. Radial displacement amplitude of monitoring points at each axial position (θ_d=0°)

To deeply understand the radial displacement response characteristics of the thin cylindrical shell with a straight crack, the radial displacement amplitude of circumferential monitoring points is extracted. According to the symmetry, the radial displacement amplitude corresponding to the other half of the circumference is complemented, which is defined as the negative phase angle. Then the radial displacement amplitude variation curves of circumferential monitoring points at axial positions *B*, *C*, *D*, *E,* and *F* are shown in Fig. 12. The radial displacement of each circumferential monitoring point along the axial direction of the straight crack shows the cosine transformation law, and the constant term of this cosine function is the radial displacement amplitude of the ideal thin cylindrical shell. By changing

the straight crack depth, it can be seen that the deeper the straight crack is, the larger the variation range of the radial displacement amplitude of the circumferential point is, and the maximum radial displacement amplitude point still well points to the circumferential position of the straight crack. But the relationship between the amplitude of different axial points is very confusing. The radial displacement amplitudes at B_0, C_0, D_0, E_0, and F_0 are extracted as shown in Fig. 13. The deeper the straight crack, the smaller the radial displacement response around the crack, which is caused by the low transmission coefficient of the vibration wave. The radial displacement amplitude increases first and then decreases with the increase of the distance from the monitoring point, and reaches the maximum near the x=2.4m. The reason for this phenomenon is that the interaction of the four waveforms of the transmitted wave reaches its maximum right here.

4.4 The straight crack identification case

The natural frequency evolution law and nonlinear vibration displacement response of the thin cylindrical shell with different crack morphology are analyzed in the above sections. With the help of the above nonlinear vibration characteristics, a straight crack identification method based on natural frequency isolines and the amplitude maximization methods is proposed. The natural frequency database of different straight crack morphology is obtained by solving the free vibration response of the thin cylindrical shell with a straight crack. The first three-order natural frequency differences corresponding to different axial positions and relative depths of the straight crack are acquired. The 3D surface diagrams of natural frequency difference are established, as shown in Fig. 14. According to the axial position and relative depth of the straight crack, corresponding points can be found on the surface diagrams of natural frequency difference of each order. Conversely, the natural frequency difference of each order can be obtained, and then corresponding isolines can be found on the surface. The axial position and relative depth of the straight crack can be obtained according to the intersection point of isolines of any two orders.

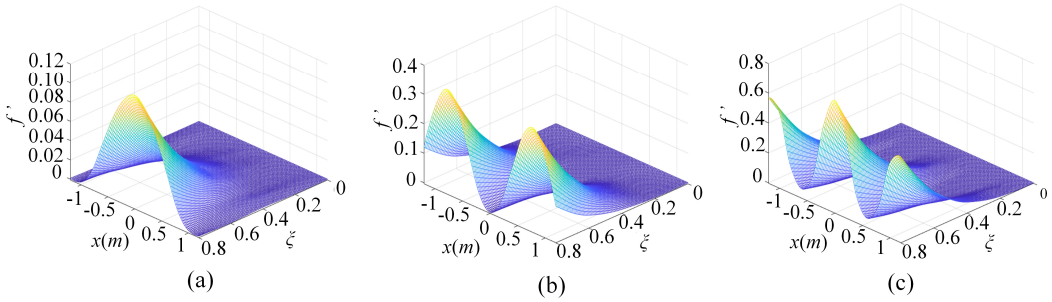

Fig. 14. The 3D surface diagrams of the first three-order natural frequency differences. (a) first-order, (b) two-order, (c) three-order.

In the identification process, the thin cylindrical shell has a high degree of symmetry. When the isolines method is used for the straight crack identification, the two isolines have completely symmetric intersection points, so the straight crack can be identified according to the side where the straight crack is located. Based on the above ideas, the straight crack is preset on the right side of the thin cylindrical shell, whose axial position is x=2.2m, relative depth is ξ=0.5, and circumferential position is θ_c=60°, as shown in Fig. 15. The natural frequency differences between the first-order and the third-order of the thin cylindrical shell with a straight crack are calculated to be $f_{\mathrm{I}}^{0}=0.026$ and $f_{\mathrm{III}}^{0}=0.136$ by FEM. Then, the corresponding isolines are obtained using these differences by intercepting the surface diagrams. These isolines can generate one intersection point, and the axial position and relative depth of the straight crack are shown in Fig 16(a). The intersection (0.502, 2.195) of the two isolines represents the axial position x=2.195m and the relative depth ξ=0.502 of the straight crack. By comparing the actual values of straight crack with the identification results, it is found that the relative error of the straight crack position is 0.125%, and the relative error of the relative depth is 0.2%. At the same time, the circumferential cosine distribution simple harmonic load is applied at x=1.0m, and the radial displacement amplitudes of the circumferential monitoring points at E are extracted. To display more intuitively, the displacement response amplitudes of each monitoring point at E are drawn into polar coordinates, as shown in Fig. 16(b). Therefore, the radial displacement amplitude of the monitoring point at θ=60° pointed by the arrow is the largest; that is, the circumferential position of the straight crack is θ_c=60°. In summary, the straight crack information obtained from the above analytical data is basically consistent with that of the preset crack, which fully proves the effectiveness of the proposed straight crack identification method. The straight crack identification method based on nonlinear displacement response characteristics and natural frequency evolution law only needs to carry out modal and displacement tests on the whole structure or local structure, which can obtain the morphology information of the straight crack and complete the straight crack identification, and effectively reducing the workload of straight crack morphology identification.

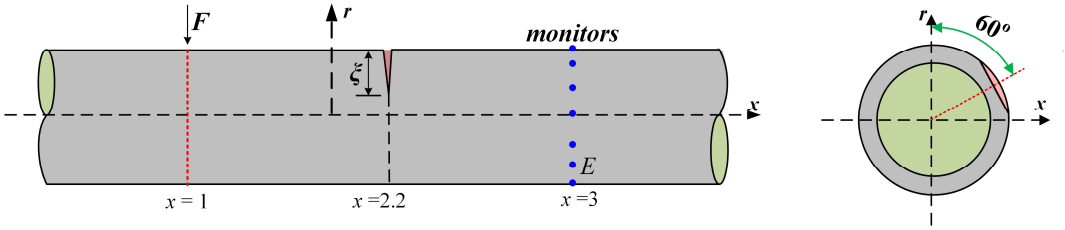

Fig. 15. Schematic diagram of preset crack

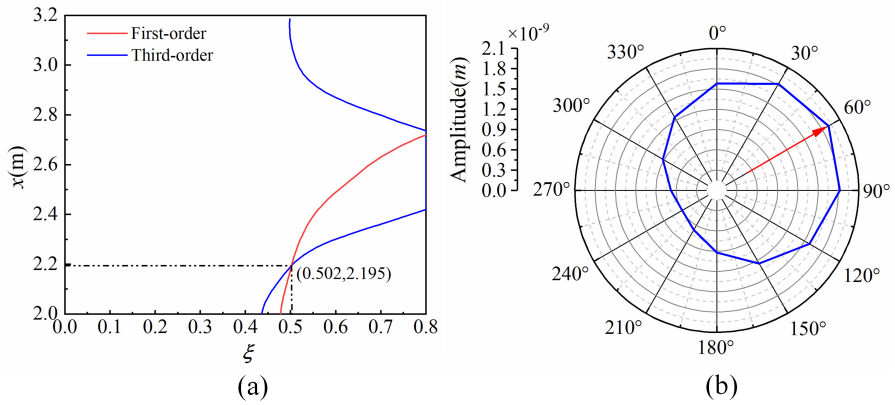

Fig. 16. Straight crack identification method. (a) natural frequency isolines intersection, (b) radial displacement amplitude.

5 Conclusion

Based on Flügge shell theory and residual theorem, this paper studies the generation and propagation mechanism of forced vibration of the thin cylindrical shell and obtains the analytical solution of forced vibration displacement in the space domain. Then, the local flexibility matrix is established using fracture mechanics theory, and the continuous coordination condition on both sides of the straight crack is constructed using the LSM. Combined with the wave superposition principle, the analytical approach for nonlinear vibration response is proposed to reveal the evolution law of nonlinear vibration response of the thin cylindrical shell with different crack morphology. The straight crack identification method based on natural frequency isolines and amplitude maximization methods is presented according to the nonlinear vibration response characteristics. The main conclusions are summarized below.

(1) The nonlinear vibration response of the thin cylindrical shell in breathing mode is affected by the propagation wave, attenuated standing wave, and near-field wave. When the characteristic equation contains real roots, as the value of the real roots increases, the acting proportion and effect of corresponding propagating waves also increase significantly, and the oscillation frequency of the displacement amplitude curve increases. When the characteristic equation contains the pure virtual roots and the value is small, the effect of the near-field wave on the displacement response is excellent, but only in the initial stage. When the number of propagation waves is more than one and more waves have similar effects in a specific direction, the displacement amplitude curve appears to be a noticeable wave superposition effect.

(2) The straight crack leads to local flexibility of the thin cylindrical shell and reduces the natural frequency of the thin cylindrical shell. The deeper the straight crack, the more strongly the natural frequency decreases. At the same time, with the increase of the order, the influence of the axial position of the

straight crack on the natural frequency becomes greater. When the straight crack is located at a certain modal node, the straight crack has almost no effect on the natural frequency.

(3) The axial and radial displacements of the thin cylindrical shell in the breathing mode can be decoupled from each other, and their radial displacement amplitudes at all points in the circumferential direction are equal. The existence of the straight crack destroys the decoupling characteristics of the axial and radial directions, resulting in obvious circumferential displacement response, but has little effect on the axial displacement. Under the excitation of circumferential cosine distribution simple harmonic load, the amplitude of radial displacement on the other side of the straight crack increases first and then decreases as the monitoring point moves away from the straight crack. The deeper the crack is, the greater the range of circumferential displacement amplitude is. The maximum radial displacement amplitude point still well points to the circumferential position of the straight crack.

(4) The unique intersection point of the natural frequency isolines of different orders can represent the axial position and relative depth of the straight crack. The radial displacement amplitude characteristics of the circumferential point under the excitation of circumferential cosine distribution simple harmonic load represent the circumferential position of the straight crack. The straight crack identification method based on natural frequency isolines and amplitude maximization methods can effectively obtain three dimensional morphology information of circumferential position, axial position and relative depth of the straight crack.

Different working conditions of the shell components can lead to complex and changeable crack morphology. This paper only makes a valuable attempt to identify the damage to the highly symmetrical straight cracked shells. It can also be applied to crack damage identification of the thin cylindrical shell under different boundary conditions. The research results provide theoretical references for straight crack identification under complex word conditions and provide a new idea for structural damage localization in machinery, chemical industry, energy, and other fields. The following research could focus on the mesoscopic crack stress release model and its solution method.

Declaration of Competing Interest

The authors declare that they have no known competing financial interests or personal relationships that could have appeared to influence the work reported in this paper.

CRediT authorship contribution statement:

Tong Wang: Conceptualization, Methodology, Software, Formal analysis, Validation, Data curation, Writing—original draft preparation, Writing—review and editing. **Chengyan Wang:** Validation, Investigation, Resources, Visualization. **Yaxing Yin:** Validation, Data curation, Writing—original draft preparation. **Yankang Zhang:** Formal analysis, Investigation, Visualization. **Lin Li:** Investigation, Visualization. **Dapeng Tan:** Conceptualization, Methodology, Project administration, Funding acquisition

Data Availability

The data that support the findings of this study are available from the corresponding author, Dapeng Tan, upon reasonable request.

Acknowledgements:

This research was funded by National Natural Science Foundation of China (Grant No. 51775501 and 52175124), Natural Science Foundation of Zhejiang province (Grant No. LZ21E050003 and LY17E050004) and Zhejiang Provincial Science and Technology Innovation Activity Program for College Students (New Miao Talent Program) (Grant No. 2021R403064)

Appendix A

The detailed expressions of coefficient matrix $[N_{3\times3}]$ are described in the following forms.

$$N_{11} = \lambda^2 + n^2\left(1+\beta^2\right)\frac{1-\mu}{2} - \Omega^2$$

$$N_{12} = -in\frac{1+\mu}{2}\lambda$$

$$N_{13} = -i\beta^2\lambda^3 - \left(i\mu - in^2\beta^2\frac{1-\mu}{2}\right)\lambda$$

$$N_{21} = in\frac{1+\mu}{2}\lambda$$

$$N_{22} = (1+3\beta^2)\frac{1-\mu}{2}\lambda^2 + n^2 - \Omega^2$$

$$N_{23} = n\beta^2\frac{3-\mu}{2}\lambda^2 + n$$

$$N_{31} = -i\beta^2\lambda^3 - \left(i\mu - in^2\beta^2\frac{1-\mu}{2}\right)\lambda$$

$$N_{23} = -n\beta^2\frac{3-\mu}{2}\lambda^2 - n$$

$$N_{33} = -1-\beta^2(n^2-1)^2+\Omega^2-2n^2\beta^2\lambda^2-\beta^2\lambda^4$$

Appendix B

The coefficient $a_i\,(i=0,2,4,6,8)$ of the algebraic equation in Section 2.1 are expressed as

$$a_0 = \left(n^2(1+\beta^2)\frac{1-\mu}{2}-\Omega^2\right)\left(n^2-\Omega^2\right)\left(-1-\beta^2(n^2-1)^2+\Omega^2\right)+\left(n^2(1+\beta^2)\frac{1-\mu}{2}-\Omega^2\right)n^2$$

$$\begin{aligned}a_2 = &\left(n^2-\Omega^2+(1+3\beta^2)\frac{1-\mu}{2}\left(n^2(1+\beta^2)\frac{1-\mu}{2}-\Omega^2\right)\right)\left(-1-\beta^2(n^2-1)^2+\Omega^2\right)\\ &-2n^2\beta^2\left(n^2(1+\beta^2)\frac{1-\mu}{2}-\Omega^2\right)\left(n^2-\Omega^2\right)+2in^2\frac{1+\mu}{2}\left(i\mu-in^2\beta^2\frac{1-\mu}{2}\right)\\ &-\left(i\mu-in^2\beta^2\frac{1-\mu}{2}\right)^2\left(n^2-\Omega^2\right)+n^2+2n^2\beta^2\frac{3-\mu}{2}\left(n^2(1+\beta^2)\frac{1-\mu}{2}-\Omega^2\right)\\ &-^2\left(-1-\beta^2(n^2-1)^2+\Omega^2\right)\left(n\frac{1+\mu}{2}\right)\end{aligned}$$

$$\begin{aligned}a_4 = &(1+3\beta^2)\frac{1-\mu}{2}\left(-1-\beta^2(n^2-1)^2+\Omega^2\right)-2n^2\beta^2(n^2-\Omega^2)\\ &-2n^2\beta^2(1+3\beta^2)\frac{1-\mu}{2}\left(n^2(1+\beta^2)\frac{1-\mu}{2}-\Omega^2\right)-\beta^2\left(n^2-\Omega^2\right)\left(n^2(1+\beta^2)\frac{1-\mu}{2}-\Omega^2\right)\\ &+2in^2\beta^2\frac{3-\mu}{2}\frac{1+\mu}{2}\left(i\mu-in^2\beta^2\frac{1-\mu}{2}\right)+2in^2\frac{1+\mu}{2}\left(i\beta^2\right)+2\beta^2\left(\mu-n^2\beta^2\frac{1-\mu}{2}\right)\left(n^2-\Omega^2\right)\\ &+\left(\mu-n^2\beta^2\frac{1-\mu}{2}\right)^2\left((1+3\beta^2)\frac{1-\mu}{2}\right)+2n^2\beta^2\frac{3-\mu}{2}+\left(n^2(1+\beta^2)\frac{1-\mu}{2}-\Omega^2\right)\left(n\beta^2\frac{3-\mu}{2}\right)^2\\ &+2n^2\beta^2\left(n\frac{1+\mu}{2}\right)^2\end{aligned}$$

$$\begin{aligned}a_6 = &-2n^2\beta^2(1+3\beta^2)\frac{1-\mu}{2}-\beta^2\left(n^2-\Omega^2\right)\\ &+\beta^2(1+3\beta^2)\frac{1-\mu}{2}\left(n^2(1+\beta^2)\frac{1-\mu}{2}-\Omega^2\right)-\beta^4n^2\frac{(1+\mu)(3-\mu)}{2}\\ &+\beta^4\left(n^2-\Omega^2\right)+2\beta^2(1+3\beta^2)\frac{1-\mu}{2}\left(\mu-n^2\beta^2\frac{1-\mu}{2}\right)+\left(n\beta^2\frac{3-\mu}{2}\right)^2\\ &+\left(n\beta\frac{1+\mu}{2}\right)^2\end{aligned}$$

$$a_8 = \left(\beta^4-\beta^2\right)\left((1+3\beta^2)\frac{1-\mu}{2}\right)$$

Appendix C

The analytical solutions of axial $u(x)$, circumferential $v(x)$, and radial $w(x)$ displacement responses are obtained using the residue theorem.

$$u(x)=\frac{\Omega^2 F_x}{2\pi\rho_s hR\omega^2}\cdot\left[2\pi i\sum_{k=1}^{m}Res[M_{13}(\lambda_k)]+\pi i\sum_{k=1}^{8-2m}Res[M_{13}(\lambda_k)]\right]$$

$$=\frac{\Omega^2 F_x}{2\pi\rho_s hR\omega^2}\cdot\mathrm{Re}\left[\left(\begin{array}{l}2\pi i\cdot\displaystyle\sum_{k=1}^{m}\frac{\alpha_1'\lambda_k^4+\beta_1'\lambda_k^2+\gamma_1'\lambda_k{}^0}{8a_8'\lambda_k^7+6a_6'\lambda_k^5+4a_4'\lambda_k^3+2a_2'\lambda_k}\\+\pi i\cdot\displaystyle\sum_{k=1}^{8-2m}\frac{\alpha_1'\lambda_k^4+\beta_1'\lambda_k^2+\gamma_1'\lambda_k{}^0}{8a_8'\lambda_k^7+6a_6'\lambda_k^5+4a_4'\lambda_k^3+2a_2'\lambda_k}\end{array}\right)\cdot\exp(i\frac{\lambda_k}{R}x)\right]$$

$$v(x)=\frac{\Omega^2 F_x}{2\pi\rho_s hR\omega^2}\cdot\left[2\pi i\cdot\sum_{k=1}^{m}Res[M_{23}(\lambda_k)]+\pi i\cdot\sum_{k=1}^{8\text{-}2m}Res[M_{23}(\lambda_k)]\right]$$

$$=\frac{\Omega^2 F_x}{2\pi\rho_s hR\omega^2}\cdot\mathrm{Re}\left[\left(\begin{array}{l}2\pi i\cdot\displaystyle\sum_{k=1}^{m}\frac{a_2'\lambda_k^4+\beta_2'\lambda_k^2+\gamma_2'\lambda_k{}^0}{8a_8'\lambda_k^7+6a_6'\lambda_k^5+4a_4'\lambda_k^3+2a_2'\lambda_k}\\+\pi i\cdot\displaystyle\sum_{k=1}^{8-2m}\frac{a_2'\lambda_k^4+\beta_2'\lambda_k^2+\gamma_2'\lambda_k{}^0}{8a_8'\lambda_k^7+6a_6'\lambda_k^5+4a_4'\lambda_k^3+2a_2'\lambda_k}\end{array}\right)\cdot\exp(i\frac{\lambda_k}{R}x)\right]$$

$$w(x)=\frac{\Omega^2 F_x}{2\pi\rho_s hR\omega^2}\cdot\left[2\pi i\cdot\sum_{k=1}^{m}Res[M_{33}(\lambda_k)]+\pi i\cdot\sum_{k=1}^{8-2m}Res[M_{33}(\lambda_k)]\right]$$

$$=\frac{\Omega^2 F_x}{2\pi\rho_s hR\omega^2}\cdot\mathrm{Re}\left[\left(\begin{array}{l}2\pi i\cdot\displaystyle\sum_{k=1}^{m}\frac{a_3'\lambda_k^4+\beta_3'\lambda_k^2+\gamma_3'\lambda_k{}^0}{8a_8'\lambda_k^7+6a_6'\lambda_k^5+4a_4'\lambda_k^3+2a_2'\lambda_k}\\+\pi i\cdot\displaystyle\sum_{k=1}^{8-2m}\frac{a_3'\lambda_k^4+\beta_3'\lambda_k^2+\gamma_3'\lambda_k{}^0}{8a_8'\lambda_k^7+6a_6'\lambda_k^5+4a_4'\lambda_k^3+2a_2'\lambda_k}\end{array}\right)\cdot\exp(i\frac{\lambda_k}{R}x)\right]$$

where α_1', β_1' γ_1', α_2', β_2', γ_2', α_3', β_3', γ_3', a_8', a_6', a_4', and a_2' are coefficient, which are given as:

$$\alpha_1'=\beta^2(1+3\beta^2)\frac{1-\mu}{2}$$

$$\beta_1'=\beta^2\left(n^2-\Omega^2\right)+\left(\mu-n^2\beta^2\frac{1-\mu}{2}\right)\left((1+3\beta^2)\frac{1-\mu}{2}\right)-\frac{1+\mu}{2}\frac{3-\mu}{2}n^2\beta^2$$

$$\gamma_1'=\left(\mu-n^2\beta^2\frac{1-\mu}{2}-\frac{1+\mu}{2}\right)n^2+\left(\mu-n^2\beta^2\frac{1-\mu}{2}\right)\Omega^2$$

$$\alpha_2'=-n\frac{1+\mu}{2}\beta^2-n\beta^2\frac{3-\mu}{2}$$

$$\beta_2'=n\frac{1+\mu}{2}\left(n^2\beta^2\frac{1-\mu}{2}-\mu\right)-\left(n^2(1+\beta^2)\frac{1-\mu}{2}-\Omega^2\right)\left(n\beta^2\frac{3-\mu}{2}\right)$$

$$\gamma_2'=-\left(n^2(1+\beta^2)\frac{1-\mu}{2}-\Omega^2\right)n$$

$$\alpha_3' = (1+3\beta^2)\frac{1-\mu}{2}$$

$$\beta_3' = n^2 - \Omega^2 + \left(n^2(1+\beta^2)\frac{1-\mu}{2} - \Omega^2 \right)(1+3\beta^2)\frac{1-\mu}{2} + in\frac{1+\mu}{2}$$

$$\gamma_3' = \alpha' f' = \left(n^2(1+\beta^2)\frac{1-\mu}{2} - \Omega^2 \right)\left(n^2 - \Omega^2 \right)$$

$$a_8' = -a_8,\ \ a_6' = a_6,\ \ a_4' = -a_4,\ \ a_2' = -a_2$$

References

1. Shi, L., Shuai, J., Wang X.L., Xu, K.: Experimental and numerical investigation of stress in a large-scale steel tank with a floating roof. Thin. Wall Struct. **117**, 25-34 (2017). https://doi.org/10.1016/j.tws.2017.03.037
2. Kolarevic, N., Nefovska-Danilovic, M.: Dynamic stiffness - based free vibration study of open circular cylindrical shells. J. Sound Vib. **486**, 115600 (2020). https://doi.org/10.1016/j.jsv.2020.115600
3. Sheng, S.S., Wang X.: The nonlinear vibrations of rotating functionally graded cylindrical shells. Nonlinear Dynam. 87(2), 1095-1109 (2017). https://doi.org/10.1007/s11071-016-3100-y
4. Mehditabar, A., Rahimi, G.H., Fard, K.: Vibrational responses of antisymmetric angle-ply laminated conical shell by the methods of polynomial based differential quadrature and Fourier expansion based differential quadrature[J]. Appl. Math. Comput. **320**, 580-595 (2018). https://doi.org/10.1016/j.amc.2017.10.017
5. Sun, S.P., Liu, L.: Multiple internal resonances in nonlinear vibrations of rotating thin-walled cylindrical shells. J. Sound Vib. **510**, 116313 (2021). https://doi.org/10.1016/j.jsv.2021.116313
6. F. W, Stresses in shells. /-2nd ed, Springer-Verlag, 1973
7. Fuller, C.R.: The effects of wall discontinuities on the propagation of flexural waves in cylindrical-shells. J. Sound Vib. **75(2)**, 207-228 (1981). https://doi.org/10.1016/0022-460X(81)90340-0
8. Sorokin, S., Manconi, E., Ledet, L., et al. Wave propagation in helically orthotropic elastic cylindrical shells and lattices. Int. J. Solids Struct. **170**, 11-21 (2019). https://doi.org/10.1016/j.ijsolstr.2019.04.031
9. Wang, Z.Q., Li, X.B., Huang, L.H.: Vibration characteristics of orthotropic circular cylindrical shells based on wave propagation approach and multi-variate analysis. J. Vib. Shock **37(7)**, 227-232. (2018).
10. Arbind. A., Reddy, J.N., Srinivasa, A.R.: A general higher-order shell theory for compressible isotropic hyperelastic materials using orthonormal moving frame. Int. J. Numer. Meth. Eng. **122**, 235–269 (2021). https://doi.org/10.1002/nme.6536
11. Zhang, G.J., Li, T.Y., Zhu, X., Yang, J., Miao, Y.Y. Free and forced vibration characteristics of submerged finite elliptic cylindrical shell. Ocean Eng. **129**, 92-106. (2017). https://doi.org/10.1016/j.oceaneng.2016.11.014
12. Guo, W.J., Li, T.Y., Zhu, X., Qu, K.Y.: Semi-analytical research on acoustic-structure coupling calculation of partially submerged cylindrical shell. Acta. Phys. Sin-Ch Ed.,

67(8), 084302 (2018). https://doi.org/10.7498/aps.67.20172681
13. Liu, Y.F., Qiu, Z.Y., Chu, F.L. Nonlinear forced vibrations of FGM sandwich cylindrical shells with porosities on an elastic substrate. Nonlinear Dynam. 104, 1007-1021 (2021). https://doi.org/10.1007/s11071-021-06358-7
14. Amabili, M., Balasubramanian, P.: Nonlinear vibrations of truncated conical shells considering multiple internal resonances. Nonlinear Dynam. 100, 77-93 (2020). https://doi.org/10.1007/s11071-020-05507-8
15. Brevart, B.J., Fuller, C.R.: Effect of an internal flow on the distribution of vibrational-energy in an infinite fluid-filled thin cylindrical elastic shell. J. Sound Vib. **167(1)**, 149-163 (1993). https://doi.org/10.1006/jsvi.1993.1326
16. Song, X.Y., Cao, T.N., Gao, P.X., Han, Q.K.: Vibration and damping analysis of cylindrical shell treated with viscoelastic damping materials under elastic boundary conditions via a unified Rayleigh-Ritz method. Int. J. Mech. Sci. **165,** 105158 (2020). https://doi.org/10.1016/j.ijmecsci.2019.105158
17. Yan, J., Li, F.C., Li, T.Y.: Vibrational power flow analysis of a submerged viscoelastic cylindrical shell with wave propagation approach. J. Sound Vib. **303(1-2)**, 264-276. (2007). https://doi.org/10.1016/j.jsv.2007.01.014
18. Mostofizadeh, S., Fagerstrom, M., Larsson, R.: Dynamic crack propagation in elastoplastic thin-walled structures: Modelling and validation. Int. J. Numer. Meth. Eng. **96(2)**, 63-86 (2013). https://doi.org/10.1002/nme.4524
19. Zhu, L.F., Ke, L.L., Xiang, Y., Zhu, X.Q.: Free vibration and damage identification of cracked functionally graded plates. Compos. Struct. **250**, (112517) 2020. https://doi.org/10.1016/j.compstruct.2020.112517
20. Nikolic, A., Salinic, S.: Free vibration analysis of cracked beams by using rigid segment method. Appl. Math. Model. **84**, 158-172 (2020). https://doi.org/10.1016/j.apm.2020.03.033
21. Naniwadekar, M.R., Naik, S.S., Maiti, S.K.: On prediction of crack in different orientations in pipe using frequency based approach. Mech. Syst. Signal Pr. **22(3)**, 693-708 (2008). https://doi.org/10.1016/j.ymssp.2007.09.007
22. Moradi, S., Tavaf, V.: Crack detection in circular cylindrical shells using differential quadrature method. Int. J. Pres. Ves. Pip. **222**, 209-216 (2013). https://doi.org/10.1016/j.ijpvp.2013.07.006
23. Zhang, Y., Lie, S.T., Xiang, Z.H., Lu, Q.H.: A frequency shift curve based damage detection method for cylindrical shell structures. J. Sound Vib. **333(6)**, 1671-1683 (2014). https://doi.org/10.1016/j.jsv.2013.11.026
24. Moazzez, K., Googarchin, H.S., Sharifi, S.M.H.: Natural frequency analysis of a cylindrical shell containing a variably oriented surface crack utilizing Line-Spring model. Thin Wall Struct. **125**, 63-75 (2018). https://doi.org/10.1016/j.tws.2018.01.009
25. Googarchin, H.S., Moazzez, K.: Analytical solution for free vibration of cracked orthotropic cylindrical shells. Int. J. Mech. Sci. **153**, 254-270 (2019). https://doi.org/10.1016/j.ijmecsci.2019.02.004
26. Pan, Z., Li, X., Ma, J.: A study on free vibration of a ring-stiffened thin circular cylindrical shell with arbitrary boundary conditions. J. Sound Vib. **314(1-2)**, 330-342 (2008). https://doi.org/10.1016/j.jsv.2008.01.008
27. Fuller, C.R.: The input mobility of an infinite circular cylindrical elastic shell filled

with fluid. J. Sound Vib. **87(3)**, 409-427 (1983). https://doi.org/10.1016/0022-460X(83)90470-4

28. Chen, G.H., Wang, T., Lu, C.D., Yang, Y.S., Li, L., Yin, Z.C., Peng, X.: Uncertainty representation of natural frequency for laminated composite cylindrical shells considering probabilistic and interval variables. App. Sci. **11(4)**, 1883 (2021). https://doi.org/10.3390/app11041883
29. Zheng, S.H., Yu, Y.K., Qiu, M.Z., Wang, L.M., Tan, D.P.: A modal analysis of vibration response of a cracked fluid-filled cylindrical shell. Appl. Math. Model. **91**, 934-958 (2021). https://doi.org/10.1016/j.apm.2020.09.040
30. Nikpour, K.: Diagnosis of axisymmetric cracks in orthotropic cylindrical shells by vibration measurement. Compos. Sci. Technol. **39(1)**, 45-61 (1990). https://doi.org/10.1016/0266-3538(90)90032-Z
31. Han, H.S., Liu, L., Cao, D.Q.: Analytical approach to coupled bending-torsional vibrations of cracked Timoshenko beam. Int. J. Mech. Sci. **166**, 105235 (2020). https://doi.org/10.1016/j.ijmecsci.2019.105235
32. Yu, Z.H., Zhang, L.B., Hu, J.Q., Hu, J.S.: Cracked modeling and vibration analysis of pipe with a part-through crack. J Vibroeng. **19(2)**, 930-942 (2017). https://doi.org/10.21595/jve.2016.17136
33. Papadopoulos, C.A.: The strain energy release approach for modeling cracks in rotors: A state of the art review. Mech. Syst. Signal Pr. **22(4)**, 763-789 (2008). https://doi.org/10.1016/j.ymssp.2007.11.009
34. Majumdar, A., Maiti, D.K., Maity, D.: Damage assessment of truss structures from changes in natural frequencies using ant colony optimization. Appl. Math. Comput. **218(19)**, 9759-9772 (2012). https://doi.org/10.1016/j.amc.2012.03.031
35. Yang, X.F., Swamidas, A.S.J., Seshadri, R.: Crack identification in vibration beams using the energy method. J. Sound Vib. **244(2)**, 339-357 (2001). https://doi.org/10.1016/0020-7683(94)90003-5
36. Lam, K.Y., Loy, C.T.: Effects of boundary conditions on frequencies of a multi-layered cylindrical shell. J. Sound Vib. **188(3)**, 363-384 (1995). https://doi.org/10.1006/jsvi.1995.0599